ELSEVIER

Journal of Nuclear Materials 313–316 (2003) 23–31

journal of nuclear materials

www.elsevier.com/locate/jnucmat

IFE chamber walls: requirements, design options, and synergy with MFE plasma facing components

A.R. Raffray [a,*], D. Haynes [b], F. Najmabadi [a]

[a] *University of California, San Diego, Fusion Energy Research Program, Mail code 0417, 458 EBU-II, 9500 Gilman Drive, La Jolla, CA 92093-0417, USA*

[b] *Fusion Technol. Inst., University of Wisconsin, 1500 Eng. Dr., Madison, WI 53706-1687, USA*

Abstract

The wall of inertial fusion energy (IFE) chambers faces demanding conditions. IFE operation is cyclic in nature and following each micro-explosion, the chamber wall is subjected to a large flux of photons, energetic particles and neutrons. Key requirements are that: (i) the chamber wall accommodates the cyclic energy deposition while providing the required lifetime, and (ii) that after each shot the chamber is cleared and returned to a quiescent state in preparation for the target injection and the firing of the driver for the subsequent shot. This paper summarizes the IFE operating conditions, discusses their impact on the choice of chamber wall configuration, and identifies the key issues. Particular attention is given to identifying common issues and operating conditions between IFE and magnetic fusion energy (MFE) with the goal of maximizing the synergy between chamber wall design and R&D for MFE and IFE.

PACS: 52.40.H
Keywords: Internal fusion; Chamber wall material; X-ray deposition; Ion energy deposition; Plasma facing components

1. Introduction

Inertial fusion energy (IFE) operation is cyclic in nature and the power plant chamber wall must accommodate the cyclic and intense photon and ion energy deposition while providing the required lifetime. Chamber concepts utilizing both solid and liquid walls have been proposed, the latter providing the possibility of armor replenishment prior to each shot. This paper assesses the requirements on chamber wall imposed by the IFE operating conditions, discussing their impact on the performance of the candidate armor materials and configurations and highlights the key issues. An underlying theme is a comparative assessment of operating conditions, armor materials and key chamber issues between IFE and magnetic fusion energy (MFE) chambers. In MFE, although some attention has recently been given to liquid armor [1], solid armor remains the main candidate on which the R&D is focused [2]. In line with this MFE emphasis and with the intent of finding the widest armor commonality between MFE and IFE, a particular emphasis is given to solid wall configurations in this paper including a discussion of operating windows. However, for completeness key issues associated with liquid walls are also discussed but to a lesser extent.

2. IFE operating conditions

In an IFE power plant, a target is first injected into the chamber. The driver (laser or heavy ion) beam is focused on the target, compressing it and initiating a fusion micro-explosion. Following each micro-explosion, the chamber wall is subjected to a large flux of photons, energetic particles and neutrons. Depending on the chamber wall loads, a background gas may be needed to

* Corresponding author. Tel.: +1-858 534 9720; fax: +1-858 822 2120.
E-mail address: raffray@fusion.ucsd.edu (A.R. Raffray).

0022-3115/03/$ - see front matter
PII: S0022-3115(02)01328-4

attenuate the energy deposition on the chamber wall by absorption and re-radiation over a longer time. The chamber has to be cleared in preparation for the injection of the next target with a typical repetition rate of about 1–10 times per second.

Two different kinds of targets are considered:

(i) A direct-drive target, illustrated in Fig. 1, whereby the driver energy is deposited directly on the target, and
(ii) An indirect-drive target, illustrated in Fig. 2, utilizing a radiation hohlraum enclosure. The X-rays resulting from the driver beam interaction with the hohlraum material is then deposited on the D-T target pellet inside the hohlraum.

The energy partitioning from two example direct-drive and indirect-drive targets (a 154 MJ NRL laser direct-drive target [3,4] and a 458 MJ heavy ion indirect-drive target [5,6]) are shown in Table 1 based on LASNEX calculations [5]. The photons and ions are the major threats to the chamber wall. Neutrons penetrate much deeper in the structure and blanket and as such are much lesser threat to the chamber wall. The corresponding photon spectra for both targets are shown in Fig. 3. The major difference between the direct-drive and

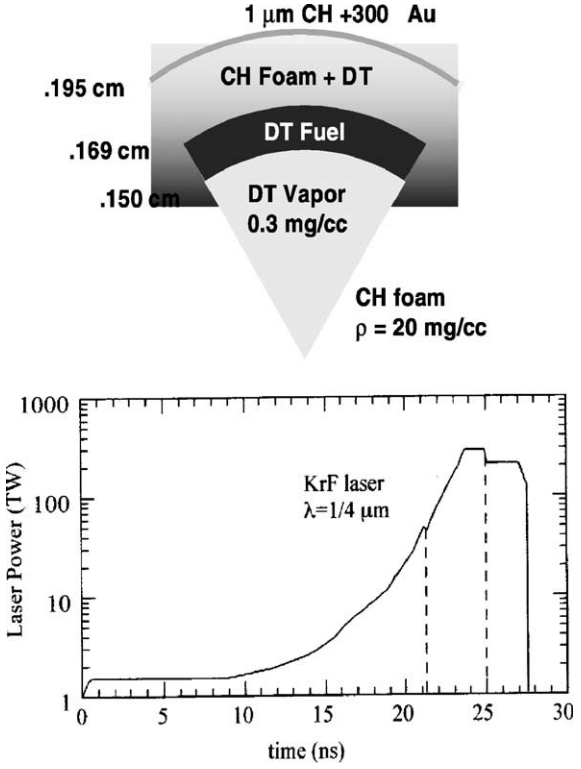

Fig. 1. Example direct-drive target (NRL) to be coupled with a laser driver [3,4].

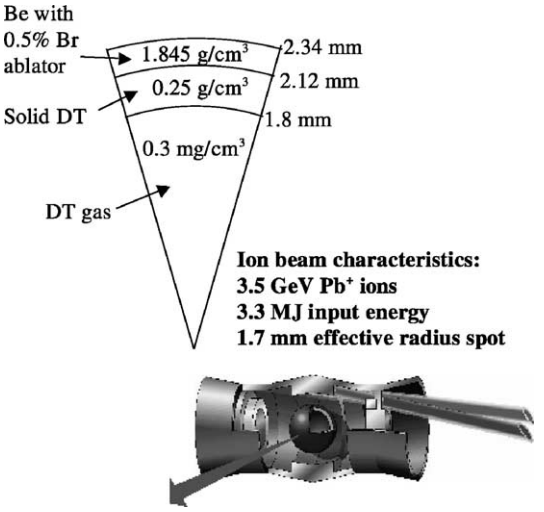

Fig. 2. Example indirect-drive target (LBLL/LLNL) to be coupled with a heavy ion beam driver [5,6].

Table 1
Energy partitioning for 154 MJ NRL direct-drive target and 458 MJ heavy ion indirect-drive target

	NRL direct-drive target (MJ)	Heavy ion indirect-drive target (MJ)
X-rays	2.14 (1%)	115 (25%)
Neutrons	109 (71%)	316 (69%)
Gammas	0.005 (0.003%)	0.36 (0.1%)
Burn product fast ions	18.1 (12%)	8.43 (2%)
Debris ions kinetic energy	24.9 (16%)	18.1 (4%)
Residual thermal energy	0.013	0.57
Total	154	458

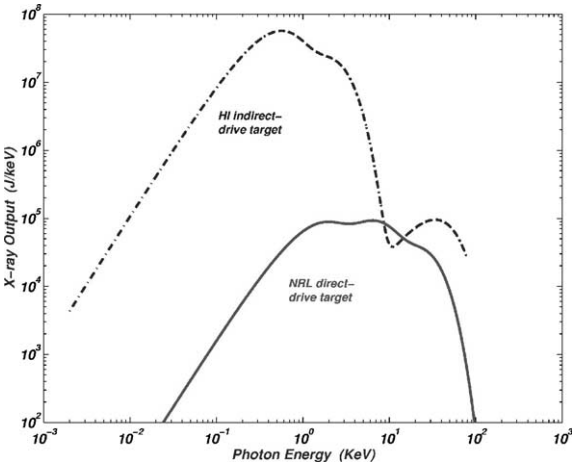

Fig. 3. Photon spectra from NRL 154 MJ direct-drive target and 458 MJ heavy ion beam indirect-drive target [5].

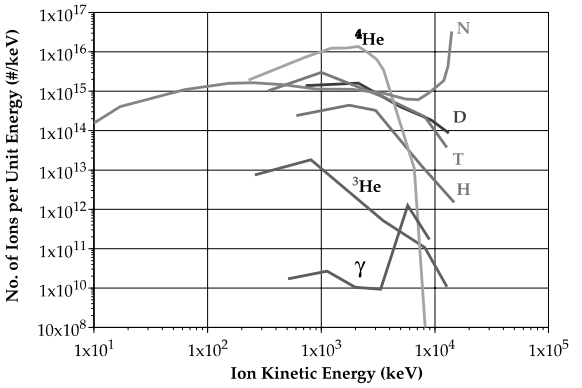

Fig. 4. Fast ion spectra from NRL 154 MJ direct-drive target [5].

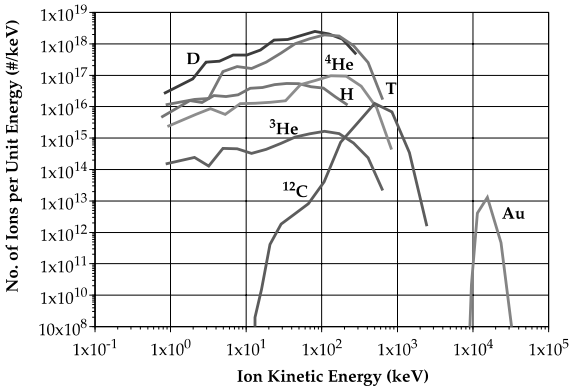

Fig. 5. Debris ion spectra from NRL154 MJ direct-drive target [5].

indirect-drive threat spectra is the huge energy component carried by photons in the indirect-drive case (25%) as opposed to the direct-drive case (1%), albeit with a softer spectrum. Photon energy deposition time is very small (typically sub ns) resulting in large heat fluxes and making it very challenging for a wall to accommodate the indirect-drive target photon threat. Detailed information on the corresponding ion spectra for both targets can be found in [5]. Here, as an example, the ion spectra for the burn products (fast ions) and the debris ions for the direct-drive target are shown in Figs. 4 and 5, respectively.

3. Dry wall armor

Candidate dry chamber armor materials must have high temperature capability and good thermal properties for accommodating energy deposition and providing the required lifetime [7]. Carbon and refractory metals (e.g. tungsten) have reasonably high thermal conductivity at high temperature (~100–200 W/m K) and high phase change temperature (sublimation temperature of carbon ~3370 °C; melting point of tungsten ~3410 °C) and are considered as candidate materials. In addition, the possibility of utilizing an engineered surface (such as a high porosity carbon fibrous carpet [8]) to maximize the incident area and provide better accommodation of high energy deposition is considered.

The energy deposition in C and W armor was calculated from the direct-drive photon and ion spectra based on a 1-D slab geometry. An attenuation calculation was used for the photon energy deposition based on data for the attenuation coefficient in the material (including photo-electric and Compton scattering effects) as a function of the photon energy [9]. The ion deposition calculation included both the electronic and nuclear stopping powers which were obtained as a function of ion energy from SRIM [10]. Fig. 6 shows an example of the energy deposition as a function of penetration depth for C and W for the direct-drive spectra assuming a chamber radius of 6.5 m and no protective gas in the chamber.

The calculation procedure included the time of flight spreading of the photon and ion energy deposition. The photons travel much faster than the ions and would reach the chamber wall within about 20 ns over a time spread of sub ns. The ions take longer to reach the chamber wall and would reach the wall at different times depending on their energy, thereby spreading the energy deposition over time and lowering the heat flux seen by the wall. As an example, a simple estimate of the ion time-of-flight based on kinetic energy is shown in Fig. 7 for the direct-drive target spectra for a case without any protective chamber gas. The fast ions reach the wall within about 0.2–1 μs whereas the slow ions reach the wall within 1–2.5 μs.

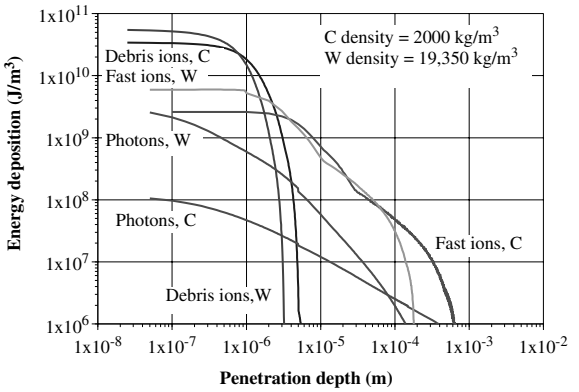

Fig. 6. Energy deposition as a function of penetration depth for 154 MJ NRL direct-drive target.

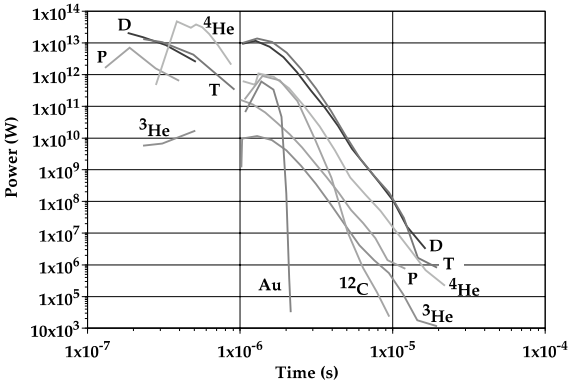

Fig. 7. Ion power deposition as a function of time for 154 MJ NRL direct-drive target.

3.1. Thermal analysis

The thermal analysis was carried out using a 1-D code based on RACLETTE [11] including melting and evaporation, and using BUCKY [12] an integrated 1-D code calculating the photon and ion energy deposition and the wall thermal response for cases with and without a protective gas. Temperature-dependent properties were utilized for both C and W; the thermal conductivity of C tends to decrease appreciably with neutron irradiation and the thermal conductivity data for irradiated C (1 dpa) were used [13].

Example results for a 3-mm W slab without a protective chamber gas is shown for a chamber radius of 6.5 m and a coolant temperature of 500 °C in Fig. 8. The major observations emerging from the results include:

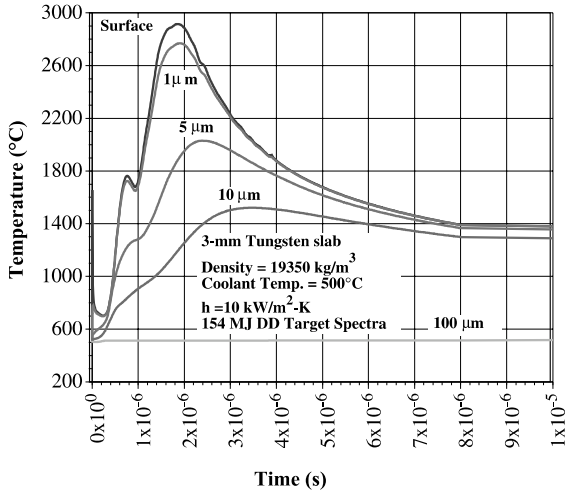

Fig. 8. Time evolution of tungsten armor temperatures at different spatial locations from the surface under 154 MJ NRL direct-drive target threat spectra.

(i) The photon energy deposition is very fast and creates an instantaneous temperature increase of about 1150 °C.
(ii) The maximum W temperature is lower than 3000 °C. It is not clear whether total melt avoidance would be required as this would depend on the stability of the melt layer and on the material form and integrity following resolidification. However, even assuming a melting point limit (3410 °C), the results indicate some margin for adjustment of parameters such as target yield, chamber size, coolant temperature and protective gas pressure.
(iii) All the action takes place in a very thin region (<100 μm) based on which a design with separate functions is preferred: a thin armor providing the high energy accommodation function bonded to a structural substrate providing the structural function and interfacing with the blanket which effectively see quasi-steady-state conditions.

Similar results were obtained for a C armor except that the initial photon-induced peak is much smaller since the photon energy deposition goes deeper inside the C and the maximum temperature is <2000 °C with an associated annual sublimation loss of less than 1 μm. From these results, a C wall can survive the photon and ion energy deposition from this target even without gas protection with some margin to allow for design optimization on various parameters.

3.2. Operating window

A number of conflicting requirements must be considered when considering an IFE chamber. In addition to wall survival with an acceptable lifetime, the coolant temperature should be maximized to increase the cycle efficiency, and the chamber size should be reasonable based on cost considerations. Inclusion of a protective chamber gas could help reduce the threat to the wall and provide the required lifetime for higher coolant temperature and/or smaller chamber size. The protective gas absorbs some of the target X-rays and ions, re-emitting the absorbed energy over longer time scales resulting in lower heat fluxes on the wall. However, the effects of the chamber gas on driver beam propagation, target injection, and target heating must be considered.

For example, thermal analysis of the direct-drive target under a given heat flux during injection indicates that the critical point of the D-T ice layer is reached with a maximum heat flux of about 6000 W/m^2 for a 400 m/s injection in a 6.5 m radius chamber (see Fig. 9). Such a heat flux can be easily achieved as it corresponds to the total radiated heat flux from a wall at 545 K or to the condensation heat flux from a Xe gas (e.g. at 1000 K and 8 mTorr, or at 4000 K and 2.5 mTorr). These parameters are well within the anticipated pre-shot conditions.

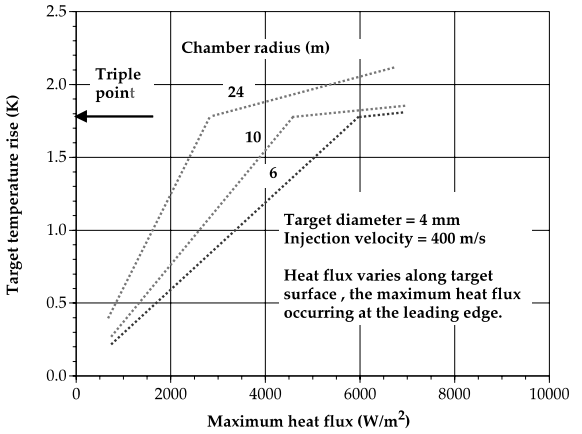

Fig. 9. Target temperature rise as a function of maximum heat flux normal at leading edge for different chamber radii.

In addition any leftover plasma at injection would result in substantial heat transfer to target through recombination. Clearly, effort is needed in this area either to better shield the target during injection or to design more thermally robust targets.

There are also requirements from the driver limiting the chamber gas density due for example to laser breakdown. As an illustration of the operating windows from these different constraints, Fig. 10 shows the maximum wall (coolant) temperature (calculated from BUCKY [12]) in a 6.5 m radius chamber corresponding to the sublimation of one molecular layer per shot as a function of the protective gas density (at RT). These results are shown as illustration as it is recognized that loss of even one atomic monolayer (~2 Å) per shot would result in unacceptably high annual armor erosion

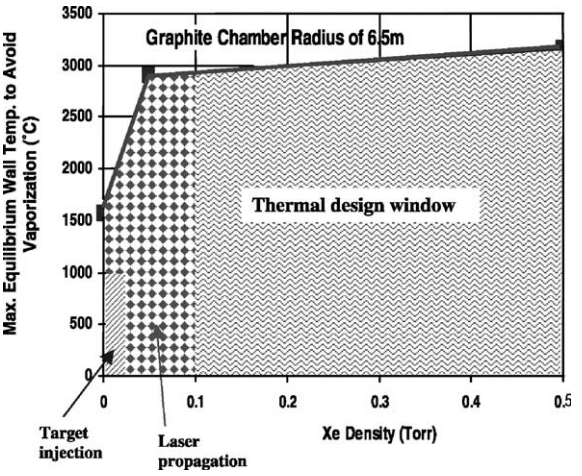

Fig. 10. Example operating design window for dry chamber wall with direct-drive target and laser driver.

(~cm's) and that a more severe constraint has to be set (e.g. assuming that so many atoms are lost per shot corresponding to a uniform average loss of a fraction of a monolayer). From the figure the thermal operating window is quite large. However, when imposing the laser breakdown constraint the Xe pressure is limited to ~0.1 Torr [14], substantially reducing the window. Consideration of target heating closes the window down even more to ~10 mTorr and ~1000 °C or less. This clearly reinforces the need to develop more thermally robust target.

3.3. Key issues and synergy with MFE chamber armor

Although the base operating conditions of IFE (cyclic operation) and MFE (with the goal of steady-state operation) are fundamentally different, an interesting parallel can be drawn between armor conditions under IFE and some MFE dynamic scenarios. For example, as shown in Table 2, the frequency, energy density and particle fluxes on the ITER divertor associated with Type 1 edge localized mode (ELM) scenarios are within about one order of magnitude of those for IFE.

Consequently and interestingly, issues driving the choice of armor material tend to be similar for MFE and IFE which provides the possibility of cross-fertilization and synergy when planning and carrying out supporting R&D. The R&D effort is focused on evolving armor material and configuration and tackling the major issues which can be broadly classified as follows:

3.3.1. High temperature and thermal stress accommodation

The armor must be able to accommodate the high energy deposition and related thermal stress without failure over the required lifetime. Of concern are the properties of the armor material at or near the melting or sublimation point. For example, a certain amount of roughnening has been observed in W under cyclic heat loads which seem to occur as the surface deforms to relieve local stresses. In the case of melting for a refractory metal (e.g. tungsten) the stability of the melt layer and the possibility of splashing must be considered.

3.3.2. Erosion

Erosion directly impacts armor lifetime. In addition, erosion in the case of MFE can create a source of impurities, which cool and dilute the plasma. In the case of IFE ablated material must be considered in the chamber clearing process to ensure that after each shot the chamber returns to a quiescent state in preparation for the target injection and the firing of the driver for the subsequent shot.

In addition to erosion due to vaporization, a number of microscopic processes must be considered in particular for carbon. These include: physical sputtering,

Table 2
Conditions assumed for ITER ELMs, VDEs and disruptions compared to conditions associated with a typical direct-drive target IFE (NRL 154MJ target) [15]

	ITER Type-I ELMs	ITER VDEs	ITER disruption thermal quench	Typical IFE operation (154 MJ direct-drive NRL target)
Energy	10–12 MJ	~50 MJ/m^2	100–350 MJ	~0.1 MJ/m^2
Affected area	5–10 m^2[a]	A few m^2[a]	~10 m^2[a]	Chamber wall (R~5–10 m)
Location	Surface (near divertor strike points)	Surface/bulk	Surface (near divertor strike points)	Bulk (~μm's)
Time	$\geqslant$ 200 μs	~0.3 s	~1 ms	~1–3 μs
Maximum temperature	Melting/sublimation	Melting/sublimation	Melting/sublimation	~2000–3000 °C (for dry wall)
Frequency	Few Hz	~1 per 100 cycles	~1 per 10 cycles	~10 Hz
Base temperature	$\geqslant$ 500 °C	~200 °C	200–1000 °C	~>700 °C
Particle fluxes	~10^{24} m^{-2} s^{-1} (peak under normal operation)			~10^{23} m^{-2} s^{-1}

[a] Large uncertainties exist.

chemical sputtering and radiation enhanced sublimation (RES). These have been studied for many years in the context of MFE and need to be applied to IFE conditions. Initial analysis suggests that RES and chemical sputtering which both increase with temperature might play an important role and should be considered [15]. Since all these processes tend to peak at ion energies of the order of 1 keV [16], their effect could be substantially increased if the IFE ion energies are drastically reduced by using a high density protective gas or by the degree of ionization of the protective gas which could substantially enhance its stopping power.

There are also macroscopic erosion processes that can be of concern, such as carbon brittle fracture and which must be better understood particularly in the IFE context.

3.3.3. Irradiation effect

Irradiation effect includes the effect of neutron irradiation on material properties and mechanical behavior and more importantly in the case of IFE of implantation of He ions in particular in W (in which He diffusion is very poor). The large fluxes of He ions can result in a 1 to 1 ratio of W:He within about 100 days of operation assuming a 1 μm implantation depth. This would lead to failure of chunks of armor and must be remedied by solutions such as operation at high enough temperature for He to be mobile in W or by using very fine porous structure providing a very short diffusion path for He to be transported to open porosity and back to the chamber.

Other irradiation issues include material activation and the associated disposal and safety concerns.

3.3.4. Tritium inventory

This includes tritium implantation and trapping in the bulk of the material and, for carbon only, co-deposition with eroded carbon redeposited in cold areas. The latter is a key concern reinforced by results from dedicated experiments and observations from current MFE devices [15]. Carbon redepostion in cold regions (< about 800 K) can lead to tritium codeposition in the ratio of up to 1:1 [17]. Although the chamber wall will be at high temperature, there are many penetration lines for the driver where the temperature will be low enough for tritium codeposition to be of concern. As part of R&D activities, techniques must be developed for removal of co-deposited T through processes such as baking, mechanical removal and local discharges.

3.3.5. Fabrication

R&D effort is needed on the fabrication of the armor material, on its bonding to a structural material, and on the armor and bond integrity under operation. In the case of IFE in particular concerns exist as to the applicability of material (and bonding) properties and behavior evolved under equilibrium or moderate transients to the highly cyclic conditions at the armor surface. Even in the most optimistic case, it is very hard to guarantee that locally the armor will not erode to unacceptable level or fail. Thus, it is imperative that in parallel with the R&D effort methods for in situ repair of the armor be developed to avoid long and costly shutdown for replacement of major wall sections in the event of local failure or erosion.

4. Liquid walls

In some cases where wall protection becomes particularly problematic such as in the case of an indirect-drive target with a high photon energy partition and hohlraum debris, use of a renewable liquid wall is attractive. The liquid wall could be used either in a thin film configuration [18] or a thick liquid jet configuration [19]. The energy deposition and particle fluxes are

accommodated by the liquid armor causing evaporation to the chamber.

A key issue is the re-establishment of the liquid wall. For a thin liquid film this must take into account re-condensation to the wall as well as re-establishment of the film by injection. The method and location of injection must be carefully designed and could be achieved either from the back through a porous medium or tangentially to the wall, or possibly with a combination of both. Major issues include the need to avoid hot spots and flow instabilities as well as to provide the required wall coverage prior to the next shot. These issues are also shared by the thick liquid wall concept where re-establishment would mostly occur through hydraulic jet control while providing the required chamber reaction pocket and penetration lines for driver and target. R&D effort in this area is applicable to both IFE and MFE configurations utilizing a liquid wall concept and is being pursued for both thin liquid film (e.g. at Georgia Institute of Technology) and thick liquid jet (e.g. at UC Berkeley and UCLA [1]).

Another important issue is the state of the chamber prior to each shot and the requirements imposed by the driver and target thermal and injection control. The chamber clearing requirements for an indirect-drive target would be much reduced because of the presence of the massive hohlraum which provides a robust thermal insulation for the target (see Fig. 2). For a heavy ion driver, depending on the mode of transport and focusing, requirements could be posed on the chamber gas and pressure. In addition, it is likely that aerosol formation would occur and it would be important to characterize the size and density of aerosol remnants prior to each shot in order to determine whether this would be acceptable for driver and target. These requirements are being assessed as part of the ARIES-IFE study [20].

Two major processes affecting the above issues are the source term for aerosol formation and the aerosol behavior between shots, and condensation to the wall. To illustrate their potential impact example results from scoping studies are presented below.

4.1. Aerosol formation and behavior

Source terms for aerosol formation include ablation of the film due to the initial high energy deposition and formation of aerosol due to in-flight condensation in saturated regions. For the indirect-drive case a large fraction of the energy is carried by photon and would reach the wall in ~10 ns. The spatial profile of this energy deposition would result in part of the wetted wall being vaporized (where the energy deposited exceeds the sensible heat + the latent heat of vaporization) but also with a 2-phase region (where the energy deposited is lower than the above case but still exceeds the sensible heat). It is not clear to what extent this 2-phase region will ablate or stay on the surface. An illustration of this 2-phase region is shown in Fig. 11 for Pb assuming the pressure of the ablated Pb at the interface is 1000 Torr.

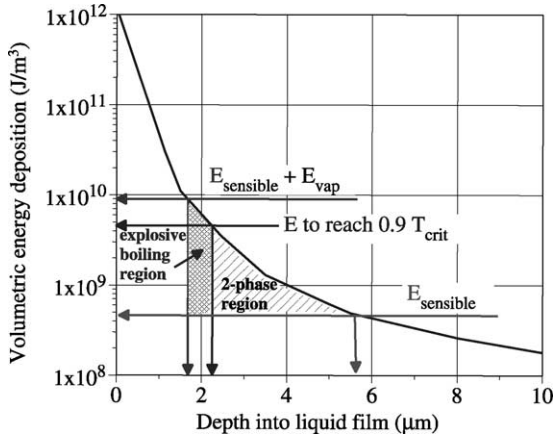

Fig. 11. Volumetric heat deposition in a Pb film from 458 MJ indirect driver photon spectra illustrating 2-phase region and regions where explosive boiling is likely to occur.

The photon energy deposition would also occur over a very short time (sub ns) giving rise to very high heating rates where, in analogy with laser ablation studies [21], the boiling mechanism would be dominated by explosive boiling instead of free surface vaporization or heterogeneous nuclei formation. The process involves rapid superheating to a metastable liquid state which has an excess free energy and decomposes explosively into liquid and vapor phases. Ref. [21] indicates that under these conditions as the temperature approaches 90% of the critical temperature and avalanche-like explosive growth in homogeneous nucleation rate (by 20–30 orders of magnitude) lead to this explosive boiling. This is illustrated also in Fig. 11 where at least the region above 90% of the critical temperature would ablate and possibly more depending on the resulting effect of explosive ablation on the surface behind.

Sources of ablated material from calculations such as these were used to estimate the aerosol formation and behavior between successive shots. Fig. 12 shows example results of the time evolution of Pb aerosol characteristics in the chamber region following a shot for a wetted Pb film for a chamber radius of 6.5 m. The initial source term was estimated from BUCKY [12] for the 458 MJ indirect-drive spectra threat. From these initial results after about 0.1 s there are still about 10^9 aerosol droplets/m^3 with sizes of about 1–10 μm. These calculations are illustrative and do not include any processes enhancing chamber clearing but indicate the potential concern of aerosol remnants that could affect the driver firing and/or target injection.

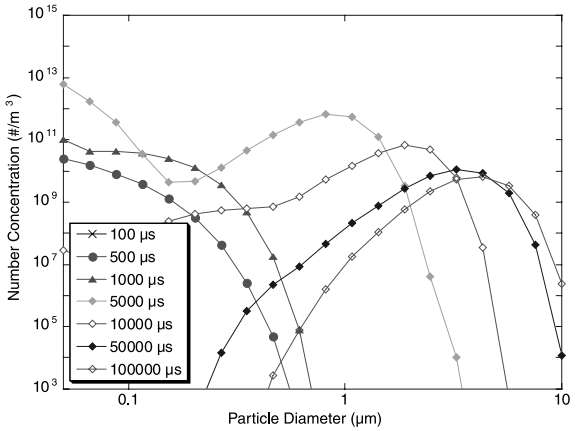

Fig. 12. Example of time evolution of Pb aerosol characteristics in the chamber region following a shot for a wetted Pb film under the 458 MJ indirect-drive spectra threat and for a chamber radius of 6.5 m.

4.2. Film condensation

Although the initial ablated mass of Pb can be estimated from calculations such as described in the previous section, it is not clear what the Pb vapor temperature and pressure would be prior to each shot as this would depend on heat transfer mechanisms and processes involved such as ionization and recombination and, very importantly, film condensation on the cooler wetted wall. As an example of the time required for condensation to clear the chamber, characteristic condensation times based on condensation rate and corresponding vapor mass in the chamber were estimated for a range of Pb vapor temperature and pressure. To be conservative, the calculations do not include the effect of vapor velocity towards the wall which can increase the condensation rate by up to a factor of ~3.6 for a velocity of the order of the sonic speed [22]. Example results are shown in Fig. 13 for a Pb film temperature of 1000 K and a chamber radius of 5 m. From the figure, the characteristic condensation time is independent of the vapor pressure until the pressure starts approaching (within about one order of magnitude) the saturation pressure corresponding to the film temperature. For all Pb vapor temperatures considered, this characteristic time is quite small (<0.04 s) compared to the time between shots (0.1–1 s) showing that condensation is fast and would probably be more limited by the heat transfer effectiveness of the wetted wall to the coolant. However, the vapor pressure prior to each shot could be higher than the film saturation pressure by up to a factor of ~10.

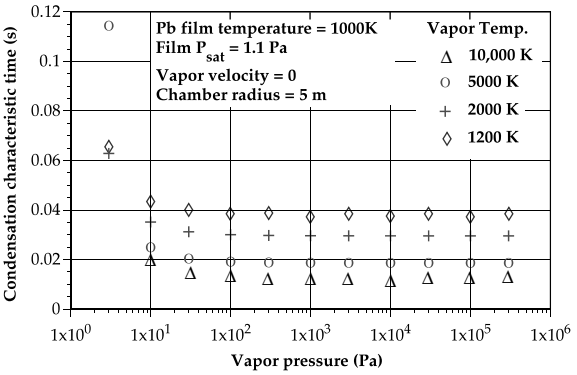

Fig. 13. Characteristic condensation time for Pb vapor as a function of vapor temperature and pressure for a film temperature of 1000 K and a chamber radius of 5 m.

5. Conclusions

The IFE chamber wall requirements of integrity, lifetime and compatibility with reactor operation are quite demanding in view of the challenging cyclic operating conditions both in terms of incident heat fluxes and particle fluxes.

Two dry wall candidate materials are carbon and refractory metals. For carbon, a major concern for the design, operation, and safety of the system is the erosion of the carbon armor over many pulses, and distribution of eroded material in combination with tritium. Refractory metals, such as tungsten, provide high temperature capability without the major tritium inventory concern. However, melting is an issue for high energy deposition and the stability of the melt layer and integrity of the resolidified material must be addressed. The effect of helium ion implantation on the armor integrity is also a key issue in particular for tungsten in which He diffusion is very slow. Operating window analysis including wall vaporization and driver and target requirements indicate that a design window exists for a laser-fired direct-drive target and a dry wall chamber. However, the window would subtantially open if a more thermally robust target can be designed.

Liquid wall configurations (thin film or thick wall) provide an alternative for cases where wall protection is problematic such as for indirect-drive targets with high photon energy and hohlraum debris. Key issues include the film or jet re-establishment, and the chamber conditions prior to the next shot in relation with the driver and target requirement. In this regard, aerosol formation and condensation are two key processes.

Although IFE operation is cyclic in nature while MFE operation targets steady state, it is interesting to see that there are dynamic MFE operation scenarios in particular for the next step device whose loading conditions on the armor show some commonality with IFE. This is particularly relevant for ELM's scenarios whose

energy density and frequency and maximum particle fluxes are within an order of magnitude of IFE operation. Thus, there is substantial overlap in the configuration and material considered for MFE and IFE chamber walls and in the related issues. This provides a fertile ground for maximizing the synergy between MFE and IFE armor R&D.

Acknowledgements

Much of the work presented here has been performed under US DOE grant number DE-FC03-95ER54299. The authors wish to acknowledge the contributions of Dr Phil Sharpe of INEEL for the aerosol calculations and of Dr Mofreh Zaghloul for the explosive boiling analysis. Also acknowledged are the helpful discussions with many members of the ARIES-IFE and High Average Power Laser Teams in the US.

References

[1] M.A. Abdou, The APEX Team, Fus. Eng. Des. 54 (2001) 181.
[2] G. Federici, C.H. Skinner, et al., Nucl. Fusion 41 (2001) 1967.
[3] D.T. Goodin et al., Nucl. Fusion 41 (2001) 527.
[4] S.E. Bodner et al., Phys. Plasmas 7 (2000) 2298.
[5] Available from <http://aries.ucsd.edu/ARIES/WDOCS/ARIES-IFE/SPECTRA/>.
[6] D.A. Callahan-Miller, M. Tabak, Nucl. Fusion 39 (1999) 883.
[7] W.R. Meier et al., OSIRIS and SOMBRERO Inertial Fusion Power Plant Designs: Final Report, WJSA-92-01 (DOE/ER/54100-1), March 1992.
[8] Available from <http://www.esli.com>.
[9] Available from <http://aries.ucsd.edu/LIB/PROPS/PHOTON/>.
[10] Available from <http://www.srim.org/>.
[11] A.R. Raffray, G. Federici, J. Nucl. Mater. 244 (1997) 85; see also G. Federici, A.R. Raffray, J. Nucl. Mater. 244 (1997) 101.
[12] R.R. Peterson et al., Fus. Technol. 30 (1996) 783.
[13] L. Snead, Oak Ridge National laboratory, USA, personal communication.
[14] J. Sethian, Naval Research Laboratory, Washington, DC, private communication, 2002.
[15] A.R. Raffray et al., ISFNT-6 presentation, Fus. Eng. Des., in press.
[16] J. Roth et al., Nucl. Fusion (1991).
[17] R. Causey, ISFNT-6 presentation, Fus. Eng. Des., in press.
[18] M.S. Tillack et al., The Prometheus Team, in: Proceedings of the 15th IEEE/NPSS SOFE, Hyannis, MA, 1993, p. 993.
[19] C. Jantzen, E. Lee, P.F. Peterson, Fus. Technol. 34 (1998) 1047.
[20] Available from <http://aries.ucsd.edu/ARIES/WDOCS/ARIES-IFE/>.
[21] W. Fucke, U. Seydel, High Temp. High Press. 12 (1980) 419.
[22] J.G. Collier, Convective Boiling and Condensation, 2nd Ed., McGraw-Hill, New York, 1981.